Direct immunomagnetic detection of low abundance cardiac biomarker by aptamer DNA nanocomplex

Wong, Ka Wang; Xu, Di; He, Dinggeng; Wong, Man Shing; Li, Hung Wing

Published in:
Sensors and Actuators, B: Chemical

DOI:
10.1016/j.snb.2019.04.035

Published: 15/07/2019

Document Version:
Peer reviewed version

Direct detection of low abundance cardiac biomarker by aptamer DNA nanocomplex

Ka-Wang Wong,[†] Di Xu,[†] Dinggeng He,[†] Man Shing Wong[*,†] and Hung-Wing Li[*,†]

†Department of Chemistry, Hong Kong Baptist University, Hong Kong

*Corresponding author e-mail: hwli@hkbu.edu.hk, mswong@hkbu.edu.hk

Abstract: An early and rapid diagnosis of acute myocardial infraction (MI) by serum biomarker quantification is vital for boosting up treatment efficacy and survival rate; however, it still remains challenging due to ultralow biomarkers content and the emergent nature of the disease. In view of these challenges, a single-step target capturing method for cardiac Troponin I (cTnI), the major cardiac biomarker of MI, was developed. The detection of target cTnI was performed by coupling the capture antibody modified magnetic silica nanoparticle ($mSiO_2$) and an aptamer-based DNA nanostructure produced by hybridization chain reaction (aptHCR). cTnI in sample was first directly captured by $mSiO_2$ and aptHCR in 30 minutes. The as formed nanocomplex was then labelled by a customized DNA turn on fluorescent dye SPM. By reading the strengthened fluorescent signal using total internal reflection fluorescence microscope (TIRFM), the detection platform has accomplished an impressive LOD of 8.5 fM with high specificity towards cTnI. The advantages of the short immunoreaction time (30 min) and the pre-treatment free property of the method have addressed the urgent diagnostic requirements of MI. The detection platform offers a potential solution to tackle insufficient sensitivity and tedious turnaround time of clinically approved assays for cTnI detection.

Keywords: Aptamer, Hybridization Chain Reaction (HCR), one step target capture, turn on fluorescent dye, cardiac Troponin I (cTnI)

1. Introduction

Acute myocardial infarction (MI), widely known as heart attack, has been a major cause of death [1]. According to data from WHO in 2015, cardiovascular diseases (CVDs) accounted for around 17.7 million deaths globally, taking up 31% of total deaths worldwide. Among these deaths, 7.4 million was contributed from coronary heart disease [2]. The prevalent disease features blockage of coronary arteries that cut down heart blood supply drastically to posse permanent heart cell damage [3]. Clinical studies have demonstrated that early invasive intervention can restrict myocardial damage to retain cardiac function and thus reducing MI patients' mortality [4,5]. Hence, early diagnosis of MI is key to treatment efficacy.

Current MI diagnostic methods include examination of symptoms, electrocardiography (ECG) ST-T wave change observation and imaging test [1,6]. These methods suffer from a range of disadvantages, such as low specificity of ECG method [7] as well as expensive [8] and long examination time [9] of MRI imaging. With the recognition of cardiac troponin I (cTnI) and cardiac troponin T (cTnT) as the "gold standard" of MI diagnosis, the disease diagnostic performance has been considerably improved [6]. The serum level of the two cardiac muscle proteins rises drastically from the onset of MI to peak at around 30 hours [10]. The unique profile of serum cardiac troponin from MI patient has enabled serial troponin analysis – measurement of serum cTnI level at multiple time points starting from the time of admission to confirm the change of biomarker level over time further enhances diagnostic performance [11]. Serial measurements method can be named as 0/x hour algorithm, which refers to sample taken at the time of hospital administration and at x hour later, or x hour delta method, which is a representation of the time difference between 0 and x mentioned above. Interestingly, recent advancements in the sensitivity of cTnI assay has potentially capacitated the implementation of 0/1-hour algorithm [12,13] or even recently a 30 minutes delta [14] method instead of the current 0/3h-algorithm [13]. The improvement in limit of detection of cTnI assay from 1.5 ng/mL in 1995 to 0.04 ng/mL in 2007 has enabled an earlier detectable signal for prompt diagnosis of the disease [10]. Recent reports of high sensitivity immunoassay (hs-cTn) has pushed the disease diagnostic cut-off value to 0.01 ng/mL, offering an earlier diagnostic start point for serial cTnI detection [8,16] and thus diagnosing MI earlier for proper treatment. Hence, detection limit, sensitivity and detection time of an assay exerts drastic influence on MI diagnostic performance. However, the common clinical cTnI detection method, enzyme-linked immunosorbent assay (ELISA), suffers from complicated procedures, such as relative long assay time and high sample consumption [17]. Taking together the low abundance nature of cardiac troponin, emergency of the disease and the practical limitations of ELISA, development

of an ultrasensitive, direct and efficient tool targeting cardiac troponin will have great impact on MI diagnostic time and hence its treatment efficacy.

To address such challenges in attaining early diagnosis of MI, herein, we have developed a single-step cTnI capturing diagnostic tool for MI (see Figure 1 for the detection strategy). The detection of cTnI was performed by capturing cTnI simultaneously by antibody modified magnetic silica nanoparticle ($mSiO_2$) and aptamer based DNA nanostructure produced by hybridization chain reaction (aptHCR) in 30 minutes. The as-formed nanocomplex was labelled by a tailor made, newly applied DNA turn-on fluorescent dye named SPM. The strengthened fluorescent signal from these specific nanosensors was measured by a total internal reflection fluorescence microscope (TIRFM), which provides higher signal-to-noise ratio than traditional fluorimeter due to the excitation of very limited fluorophores by its highly restricted evanescent field of around 300 nm in depth [18]. The detection platform has achieved an impressive LOD of 8.5 fM with high specificity towards cTnI.

Comparing with traditional ELISA, the developed assay utilized antibody conjugated magnetic nanoparticle to enjoy higher sensitivity [19] and shorter reaction time [20]. This is beacuse nanoprobes serves as a pre-concentrating platform and target was captured in a freely dispersion mode. Moreover, the magnetic property of nanoparticle allows easy separation of target from sample matrix. Furthermore, the amplification technique, hybridization chain reaction (HCR), allows controllable growth of a long chain DNA by sequential hybridization of single stranded DNA initiator with two types of self-hybridized hairpins at isothermal condition. This triggers a series of hairpin openings and thus efficiently generating a sizable linear DNA amplification unit [21,22]. By extending the other end of the initiator with a cTnI aptamer, an oligonucleotide sequence with high binding affinity to specific target (K_d = 270 pM towards cTnI for the aptamer adapted here)[23], the aptHCR serves dual functions in providing specific binding with cTnI and DNA based amplification. The combination of $mSiO_2$ as capture probe and aptHCR as a linear amplification unit with appropriate size offers several advantages. The concurrent cTnI capture by both $mSiO_2$ and aptHCR shortened the immunoreaction time to 30 minutes. The size controllable nature of HCR also enables the growth of DNA amplification unit with appropriate size relative to the nanoprobe and target by simply altering the initiator to hairpin ratio. Using the DNA turn-on fluorescent dye SPM to label the HCR amplified samples, a signal growth of 3.8 folds by TIRFM has been achieved compared with the cTnI absent sample. This demonstrates that the application of HCR as amplification technique coupled with efficient DNA fluorophore generated a sensitive detection platform for quantification of cTnI in early stage.

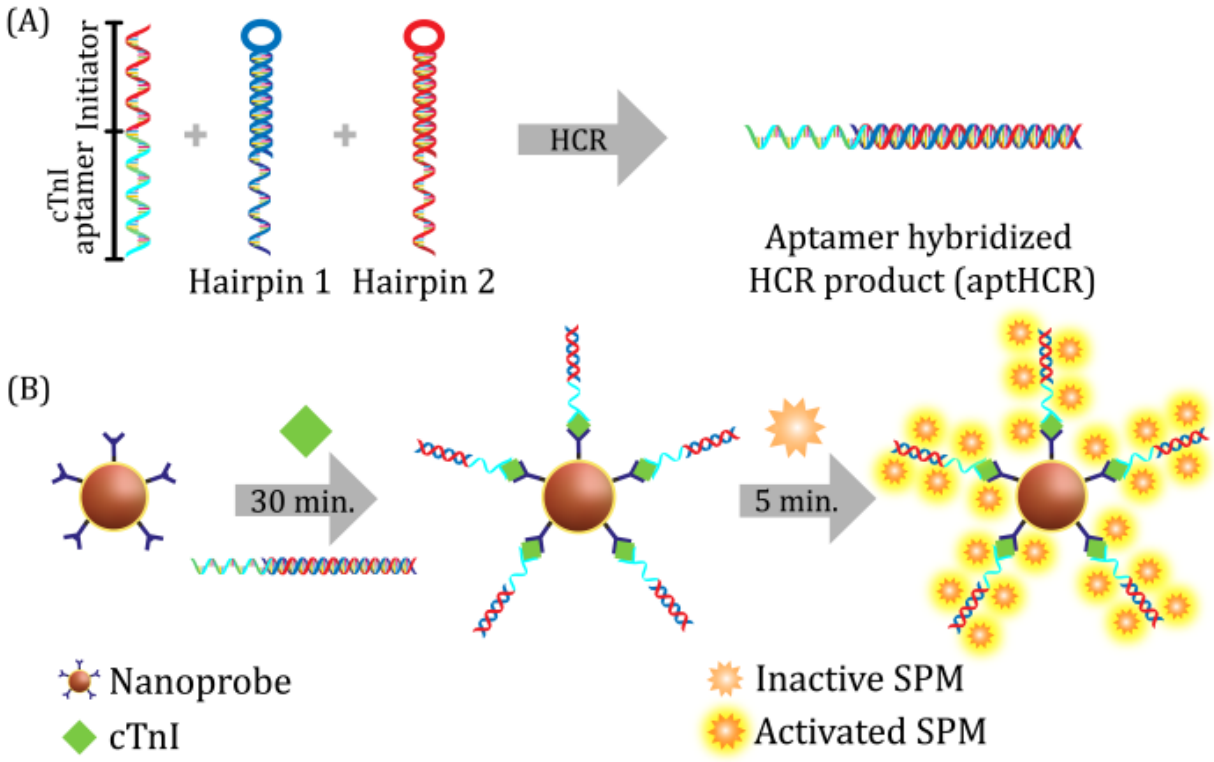

Figure 1. Schematic diagram illustrating the principle of the detection platform. (1). cTnI aptamer extended initiator was incubated with hairpin 1 and 2 to produce a long chain of aptHCR. (2). In the presence of cTnI, cTnI capture antibody conjugated nanoprobe and aptHCR simultaneously sandwiched cTnI in one step. The subsequent washing step washed away components not specifically bound on the nanoprobe. All samples were labelled by the customized DNA turn on fluorescent dye SPM.

2. Experimental Session

2.1. Construction of nanoprobe

1 mg of silica coated iron oxide nanoparticle was stirred with 100 µL (3-aminopropyl)triethoxysilane (APTES) in ethanol at 70 °C for 24 hours. After washing with distilled water for 3 times and dispersed in water, the nanoparticles were fabricated by 40 µL of 70% glutaraldehyde (GA) solution by sonicating at room temperature for 1.5 hours. The nanoparticle was washed twice by distilled water and dispersed in PBS. The activated nanoparticles were next reacted with 50 nM of capture antibody (19C7) by shaking at room temperature for 2 hours. The capture antibody immobilized nanoparticles were washed 3 times and dispersed in PBS.

2.2. Hybridization of aptamer hybridized HCR nanocomplex (aptHCR)

T4, H1 and H2 in hybridization buffer were separately heated at 92 °C for 2 minutes and cooled to room temperature for 1 hour. Then, the three solutions were combined to yield 50 µL of DNA mixture with 20 nM T4, 200 nM H1 and H2 (initiator: hairpin = 1:10). The mixture was then incubated at 78 °C for 1 hour. The as formed aptHCR was diluted by hybridization buffer to desired concentration before use.

2.3. Quantification of cTnI by TIRFM

Using the optimized conditions, cTnI was detected by TIRFM. The calibration curve of cTnI was prepared by incubating 0, 20, 50, 100, 400, 700, 1000 and 1200 fM cTnI with 0.2 mg/mL nanoprobe and 100 pM aptHCR in a total volume of 50 µL. For real sample analysis, 5 µL of human serum sample was incubated with the reaction cocktail for detection. In the test of HCR effect demonstration, accumulating sequentially, nanoprobe only sample, with 1.2 pM cTnI sample, amplified with 100 pM aptamer sample, amplified with 100 pM aptHCR sample instead of aptamer and amplified with 100 pM MF4 replacing aptHCR samples were prepared. For control samples of amplified HCR and MF4, they were prepared without cTnI in same condition. In specificity test, 1.2 pM cTnI and 12 pM of cardiac proteins cTnC and cTnT as well as 12 pM of other serum protein including BSA and IgG were separately incubated with the detection system.

All prepared reaction mixtures were incubated at 37 °C for 30 minutes. Then, all samples were labelled by 250 µM SPM for 5 minutes. The labelled samples were washed by PBS for 1 time and redispersed in 50 µL in PBS for detection. Subsequently, samples were injected into a flow cell and magnetically attracted to the cover slide for 5 minutes prior to TIRFM imaging.

2.4. TIRFM setup and data processing

The homemade setup of the prism type total internal reflection fluorescence microscope was published previously [24]. The flow cell was inserted between a fused silica isosceles prism (CVI, laser USA) and a 60X oil type objective fixed on an IX71 inverted microscope from Olympus. A 488 nm diode laser (Newport, USA) was employed as the excitation source for SPM labelled sample. Emission light was filtered by a BLP-488R long pass filter (Semrock, USA) to reach the Electron Multiplying Charge Coupled Device (EMCCD) (PhotonMax 512, Princeton Instrument, USA). The exposure time was set as 100 ms for both the shutter and the detector, which was set in frame transfer and external synchronization mode. Gain of the EMCCD was set at 4000 while the delay time of the shutter drive was 10 ms. In each region of interest within one channel, 20 sequential frames per image were taken by the manufacturer's software WinSpec/32 (version 2.5.22.0, USA). Given one light spot refers to one nanoprobe, approximately 5 images that contain more than 50 nanoprobes were recorded.

Data processing of images were conducted through the public domain image analysing software Image J (version 1.15u, NIH, USA). The average net intensity of a sample in quantification of cTnI was computed by measuring 50 bright spots with the formula: [50x(1x1 square pixel from one nanoprobe) – 50x(1x1 square pixel of individual background signal from the image)]/50. All TIRFM based experiment was conducted in triplicate with error bar referring to standard error of mean.

3. Results and Discussion

3.1. Fluorescence turn-on dye for efficient labelling

To provide an efficient signal reporting for aptHCR, a fluorescence turn-on cyanine dye, SPM was identified for aptHCR labelling [25], which affords high sensitivity in a detection assay. The molecular structure of SPM is shown in Figure 2. The planar carbazole moiety of SPM ensures a strong stacking interaction with dsDNA via intercalation and the positive charge on the dye provides an additional electrostatic interactions with negatively charged DNA. Despite its very low fluorescence quantum yield in PB (0.02), SPM exhibits a strong fluorescence enhancement upon binding with dsDNA which provides an ideal turn-on mechanism for labelling of DNA-based aptHCR [25]. Moreover, the broad band absorption property of a molecular dye provides flexible excitation of the labelled immunocomplex using commonly available lasers in general laboratory setting (Figure S2). In addition, the large Stokes shift of 148 nm from 433 nm to 581 nm (Figure S2) with high solubility in aqueous solution makes SPM a desirable candidate as a reporter for this assay. As compared with the previously employed dye, SLACE (Figure S3) [26], SPM showed an excellent turn-on property towards aptHCR with a 7.4-fold fluorescence enhancement, which was much higher than that of 1.5 folds from SLACE, upon binding with aptHCR. This indicates that SPM substantially improved the signal output of the assay.

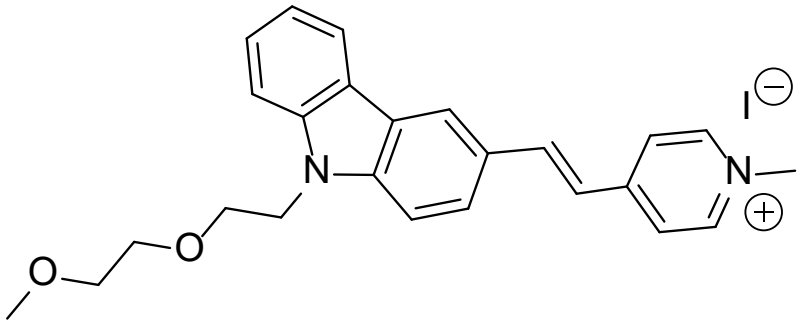

Figure 2. Chemical structure of the turn-on fluorophore, SPM.

3.2. Characterizations of the detection platform

The as-prepared silica coated iron oxide nanoparticles used in this study was characterised by a TEM (Tecnai G^2 20 S-TWIN, USA). The TEM image was shown in Figure S5A. It was demonstrated that the nanoparticles were spherical and monodispersed. Using the image processing programme imageJ (version 1.15u, NIH, USA), the average size of the nanoparticles was measured to be 329.7 ± 23.2 nm (n=100). To reveal the magnetic property of the synthesized $mSiO_2$, as displayed in Figure S5B and S5C, the originally dispersed nanoparticles in aqueous solution were attracted to the magnet to give a clear solution.

We rationally design the sequences in the hairpin system to equip aptHCR with both protein binding and signal amplifying ability by extending a cTnI aptamer with the initiator of a HCR system. Xie et al. have demonstrated that an HCR system using a poly-A spacer to connect an aptamer at the 3' end and the initiator adapted in this project at the 5' end works well for detection of lipopolysaccharides [27]. Meanwhile, Jo et al. have reported that the high affinity cTnI aptamer Tro4 can be extended at the 5' end for sensitive detection of the target [28]. Hence, the HCR initiator sequence was employed as a 5' extensor of Tro4 to give ideal target binding and HCR extending abilities. To avoid the possible formation of stem and loop structures intra initiator (AAAC and TTTG if poly-A spacer was applied), the poly-A spacer has been modified by a poly-T spacer for better HCR initiating ability. We tested the effective formation of DNA product using polyacrylamide gel electrophoresis (PAGE) to observe the size of the precursors and aptHCR. Referring to Figure S6, despite the fact that the initiator to hairpin ratio was increased from 1: 2.5 (reported in the literature) to 1: 10 (in this study), that lane 5 (aptHCR) displaying a band with obvious electrophoretic shift compared with its precursors shown in lane 2 (initiator), lane 3 (hairpin 1) and lane 4 (hairpin 2) indicated the successful formation of a long DNA amplification unit.

3.3. Amplification effect of aptHCR

To testify the amplification effect of aptHCR, samples were sequentially prepared by adding up buffer solution, cTnI, aptamer and aptHCR for examination under TIRFM. Referring to Figure 3, net average fluorescence intensity of

nanoparticles increased slightly from the sample of probe-only to target captured nanoprobe and slightly further to the aptamer amplified one. With aptHCR amplification, the signal was elevated by 2.7 times compared with the aptamer binding sample. The obvious signal increase has proven the successful amplification by the aptHCR owing to binding of the long chain DNA complex with the target. In addition, aptHCR was proven to be valuable by comparing the performance of the detection system amplified by a cTnI detection antibody (MF4). With reference to the same graph, after subtracting their control's signal, the aptHCR amplified system yielded a 5.2-fold increment compared with the MF4 one, illustrating that the capture antibody-aptHCR system outperformed the traditional sandwiched antibody one because of the large molecular weight of aptHCR as well as the strong fluorescent response of SPM towards DNA. All in all, the capture antibody-aptHCR based nanoprobe design armed the detection platform with powerful sensitivity.

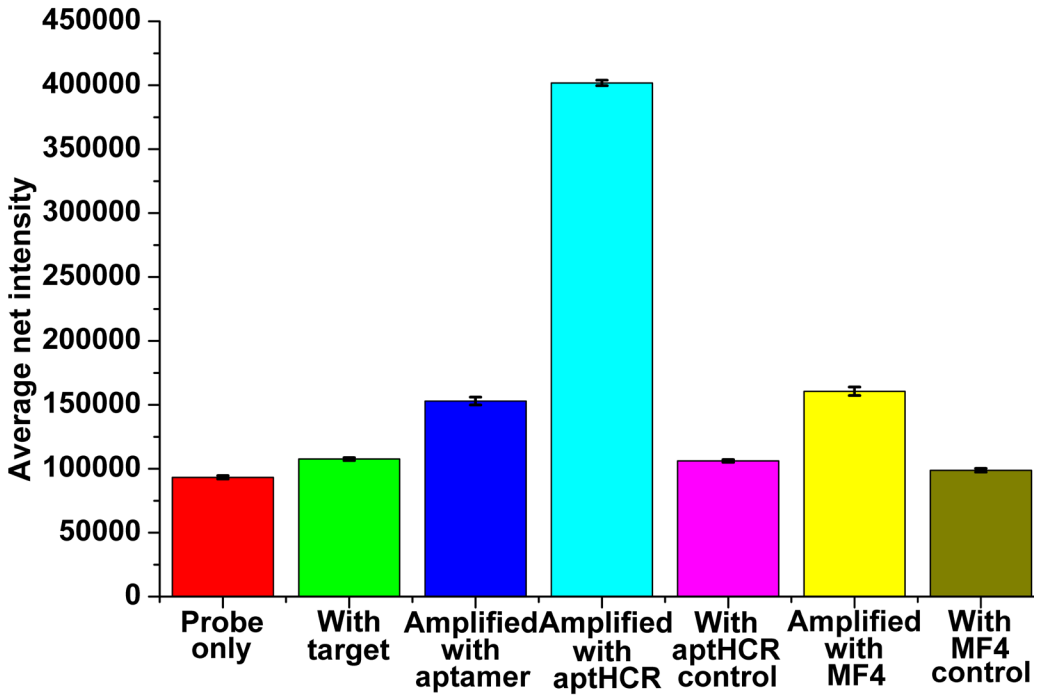

Figure 3. Effect of HCR amplification effect using aptHCR amplified immunocomplex to compare with samples adding up probe only, target cTnI captured probe, immunocomplex amplified with aptamer and cTnI detection antibody MF4 amplified immunocomplex. cTnI was absent in with aptHCR control and with MF4 control samples to compare with amplified with aptHCR and amplified with MF4 samples respectively. Error bar refers to standard error of mean with n = 3. Average net intensity was computed by the equation [20x(1x1 square pixel from one nanoprobe) – 20x(1x1 square pixel of individual background signal from the image)]/20.

3.4. Assay optimizations

To further sharpen the sensitivity of the detection platform to femtomolar level, a series of optimization experiments were designed to identify the optimal condition that gave the highest net fluorescence signal. First, to ensure saturated conjugation of capture antibody on the surface of $mSiO_2$ to provide maximum target capture capacity of the probe, a range of concentrations of capture antibody were reacted with fixed concentration of nanoparticles. Referring to Figure S7A, a gain of net signal was observed from 0.01 nM to 50 nM. Further increase in antibody concentration from 50 nM to 100 nM kept the net signal statistically equivalent. The results revealed that 50 nM of capture antibody was enough to saturate the surface of nanoparticle. Next, in an endeavour to ensure the aptHCR concentration was adequate for 500 fM cTnI, 5 - 400 pM HCR complex were reacted with the cTnI captured probe. As displayed in Figure S7B, 100 pM of the amplification unit was competent to fully amplify the target. To ensure the complete capturing of target by the antibody onto the nanoprobe, an array of reaction times from 15 minutes to 60 minutes were tested. Results displayed in Figure S7C revealed that 30 minutes was enough for the capture antibody to bind with the target. The same strategy was implemented to investigate the effect of reaction time between the target and the aptHCR to ensure complete binding. As shown in Figure S7D, 30 minutes was also enough for the

aptamer to bind with the target. The immunoreaction in the above reaction time optimizations was conducted in 2-step in that the nanoprobe target reaction and the target aptamer reaction were run separately. To look into the feasibility of the assay to be conducted in 1-step, which is, incubating the target with nanoprobe and aptHCR at the same time, the performance of 1-step and 2-step immunoreaction systems were compared. Referring to Figure 4, the fluorescence signal from 1-step reaction and the 2-step one was statistically equivalent, allowing the immunoreaction time of the assay to be cut down from 1 hour to 30 minutes. This 1-step immunoreaction would flavour the urgent nature in MI detection.

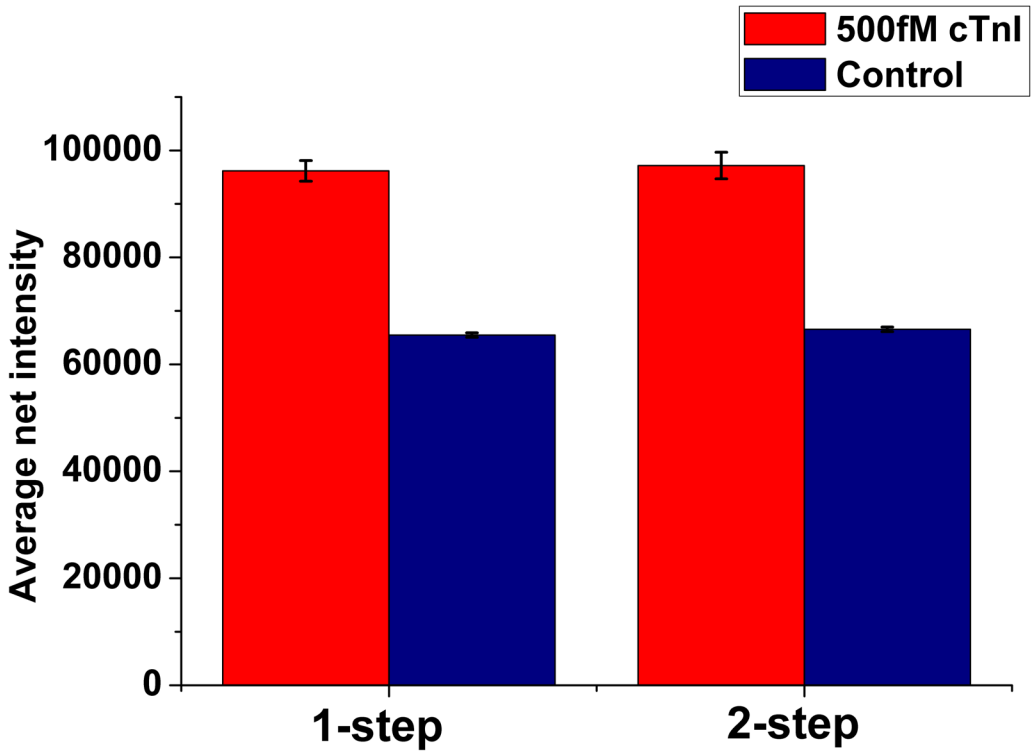

Figure 4. Effect of number of immunoreaction step. 1-step method refers to incubating the nanoprobe and aptHCR at the same time for 30 minutes while 2-steps method refers to first incubate nanoprobe with 500 fM of cTnI for 30 minutes and further react with aptHCR for extra 30 minutes. Error bar refers to standard error of mean with n = 3. Average net intensity was computed by the equation [20x(1x1 square pixel from one nanoprobe) – 20x(1x1 square pixel of individual background signal from the image)]/20.

To adjust the nanoprobe concentration for detecting low concentration sample, nanoprobe concentrations of 5, 1, 0.2 and 0.04 mg/mL were reacted with 500 fM of cTnI. As shown in Figure S7E, decreasing the nanoprobe concentration from 5 mg/ml to 0.2 mg/ml yielded an obvious increment in signal difference between the control sample and the target captured sample. The results indicated that scaling down the total amount of nanoprobe allows more target to be captured per nanoprobe and hence higher fluorescence brightness per nanoprobe. In practice, raising the nanoprobe concentration can extend the linear range of the detection platform, offering high flexibility in development of detection protocols to meet samples' need. With fewer nanoprobes, each nanoprobe's light intensity is more responsive and sensitive to target in low concentration. Further reducing the nanoprobe concentration from 0.2 mg/ml to 0.04 mg/ml maintained the net signal. To enhance the efficiency in data analysis, 0.2 mg/ml of nanoprobe was chosen to provide reasonable counts of bright spots per each TIRFM image.

In an effort to confirm the nanosensor was being labelled by optimal concentration of SPM, a series of SPM concentrations were employed to label the immunoreaction products. With reference to Figure S7F, fluorescence signal from nanosensors of the target sample gained with elevating SPM concentration while signal from the control sample also surged with SPM'S concentration in general. The largest signal difference between the target sample and its control lies in 100 µM, which is suggested to be the adequate amount of SPM used to label the target captured nanosensors with relatively low background. Further increasing dye concentration to 1 mM remained more free dye in the bulk solution, which contributed to higher background signal and hence lower average net intensity.

3.5. Direct quantification of cTnI in human serum sample

To directly quantify cTnI in heathy human serum sample, an external calibration curve for cTnI with high linearity was established. As displayed in Figure 5, the external calibration curve was set up in the range of 0 – 1200 fM with correlation coefficient of 0.9995. It was demonstrated that the linear range saturates at 1200 fM (Figure S8). The impressive LOD of 8.5 fM (0.20 pg/mL) calculated by the equation: Blank + 3x(standard deviation) of the calibration curve enabled direct detection of cTnI in heathy serum sample, which ranges from 1.1 to 7.9 pg/mL [29]. To demonstrate its feasibility in direct quantification of cTnI in serum sample, a serum sample from a heathy donor was found to contain 2.35 pg/mL of cTnI by the developed detection platform, which was within the reported range for heathy subject.

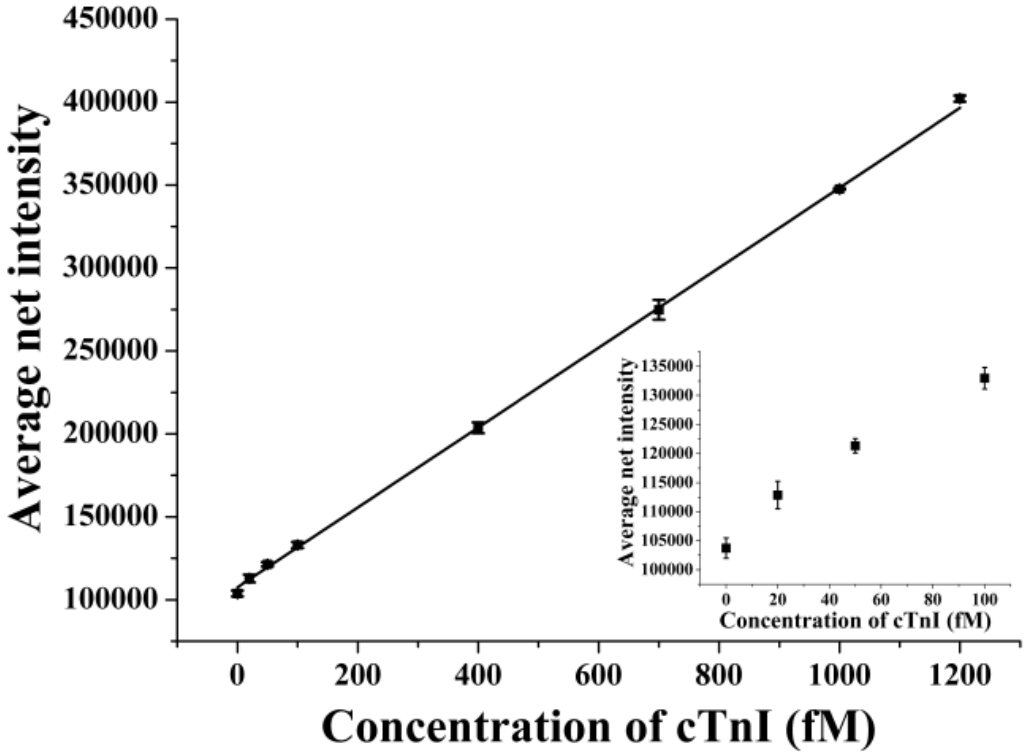

Figure 5. External calibration curve for cTnI constructed by TIRFM in the range of 0 – 1200fM cTnI. Inset displayed calibration curve in the range of 0 – 100 fM. Correlation coefficient for the curve was 0.9995. Error bar refers to standard error of mean with n = 3. Average net intensity was computed by the equation [50x(1x1 square pixel from one nanoprobe) – 50x(1x1 square pixel of individual background signal from the image)]/50.

3.6. Specificity of the detection platform

We tested the specificity of the developed method in differentiating the target protein from other serum proteins. The analysis was performed by comparing the signal of 1.2 pM of cTnI, 12 pM of two other cardiac isoforms that exist in serum sample – cTnT and cTnC and 12 pM of BSA and IgG. As shown in Figure 6, attributed to the specific interaction between the capture antibody 19C7 and cTnI, all matrix components contributed non-significant signal which is close to the blank control even in 10 times higher concentration. The cTnI reacted sample generated average net intensity significantly higher than those of the interference components, proving the high specificity of the detection platform.

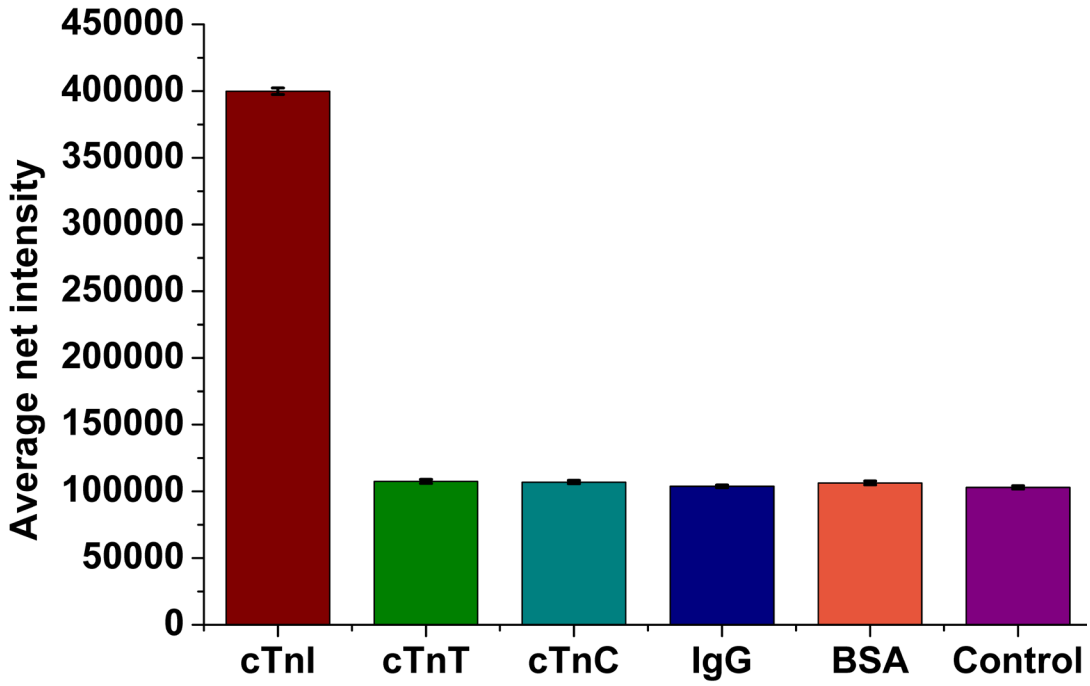

Figure 6. Specificity test for the detection method. 1.2 pM of cTnI and 12 pM of cTnT, cTnC, BSA, IgG were separately incubated with the detection platform. Error bar refers to standard error of mean with n = 3. Average net intensity was computed by the equation [20x(1x1 square pixel from one nanoprobe) – 20x(1x1 square pixel of individual background signal from the image)]/20.

3.7. Validation of the detection assay

We validated the detection platform by commercial ELISA to demonstrate the capability of the detection platform to reliably quantify cTnI in human serum sample. As summarized in Table 1, in a 2390 pg/ml (100 pM) cTnI spiked human serum sample, the TNNI3 ELSIA reported target protein level of 2581 pg/ml with recovery rate of 108% while that of TIFM was 2463.4 pg/ml with recovery rate of 103%. The small relative percentage difference (RPD) -4.6% between the two methods validated the reliability of the developed TIRFM assay.

A standard addition calibration curve was also established to validate the serum cTnI level detected by the external calibration method. As demonstrated in Figure S9, cTnI concentration of 0 – 10 pM was spiked in serum sample of a heathy donor and diluted by 10 times in accordance with assay procedure for analysis. Correlation coefficient for the curve was 0.9996. As depicted in Table 1, the serum cTnI concentrations detected by the two calibration methods were comparable. The external calibration method yielded a level of 2.35 pg/mL while the standard addition method gave a concentration of 2.47 pg/mL of cTnI in the serum sample. The insignificant RPD of -4.9% demonstrated that matrix components from the serum have little influence on the specificity of the detection platform towards cTnI.

3.8. Fluorometer assay

To testify the applicability of the detection assay in general laboratory setting, we demonstrated the analysis of cTnI using a bench-top commercial fluorometer. As shown in Figure S10, a calibration curve with cTnI ranging from 0 – 1200 fM was constructed by measuring the emission signal of the samples by a fluorometer (Horiba FL3C-21, USA). With reference to Table 1, using the established calibration curve, the 2390 pg/ml (100 pM) spiked human serum sample was found to contain 2614.4 pg/mL cTnI, which differs from the commercial ELISA one by just 1.3%. Therefore, the results supported on the reliability and accuracy of the detection strategy to practice clinically.

100 pM (2390 pg/mL) spiked serum sample:	cTnI concentration (pg/mL)	Recovery (%)	RPD (%)
TIRFM	2463.4	103	- 4.6
TNNI3 ELISA	2581	108	/
Fluorometer	2614.4	109.4	+1.3
Serum sample from heathy control:			
External calibration	2.35	n/a	-4.9
Standard addition	2.47	n/a	

Table 1. Comparisons of results obtained among the developed TIRFM detection platform, TNNI3 ELISA and fluorometer-based assay as well as external calibration and standard addition method.

4. Conclusions

Based on the application of $mSiO_2$, aptHCR, SPM and TIRFM, the detection platform has achieved superior performance. The careful deign of long nucleic acid amplification unit coupled with efficient DNA turn on dye SPM using TIRFM as signal readout has equipped the detection platform with impressive LOD of 8.5fM (0.20 pg/mL), which is well below the serum cTnI range of heathy subject ranging from 46.0 fM to 330.5 fM [29]. With a fixed dilution factor of 10X, the linear range from 20 fM to 1.2 pM covers the general cTnI cut-off value 1.26 pM [30] and even the potential sex specific cut-off value; men, 1.4 pM [31,32]; women, 670 fM [31,32] with low consumption of 5-µL serum sample. In view of the fact that elevation of serum cTnI level in heathy individual increases the risk of MI development [33,34], the ultrasensitive assay can serve as an alternative for prognosis, early and accurate diagnosis of the life-threatening MI. Coupled with the highly precise nature of this assay (R^2 = 0.9995 in external calibration curve), the developed method offers potential implementation of the faster 0/1-hour algorithm [12,13] or even the 30 minutes delta [14] method instead of the current 0/3h-algorithm [13] for clinical MI diagnosis by offering the power to precisely observe the small changes of serum cTnI level within 1 or 0.5 hour and thus shortening the total diagnostic time. In addition, the outstandingly short immunoreaction time of 30 min. of the nanosenor empowered by the high affinity of the capture antibody and aptamer, their ability to sandwich the target in one step and required only one washing step significantly cut down the turn-around time of the assay. Meanwhile, the low sample consumption (5 µL) and the low cost per sample analysis (USD $0.20, calculated by total reagent cost over number of sample able to detect) expanded the possibility for commercialization. With the capability to differentiate cTnI form serum sample matrix as well as results being validated by a commercial ELISA kit, the ultrasensitive, precise, rapid, simple, specific and economic detection platform have huge potential to be developed into a MI early detection tool by meeting the strict diagnostic requirements of the disease. In principle, the detection strategy is universal to other protein based detection as long as specific and effective antibody-aptamer pair is available.

Appendix A. Supplementary data

This material is available free of charge via the Internet at http://

Acknowledgements

Funding: This work was supported by the Cooperative Research Fund of Hong Kong Research Grant Council [C2012-15G], the General Research Fund [12301317], and the National Natural Science Foundation of China [No. 21675135].

References

[1] K.Thygesen, J.S.Alpert, A.S.Jaffe, M.L.Simoons, B.R.Chaitman, H.D.White, H.A.Katus, F.S.Apple, B.Lindahl, D.A.Morrow, P.M.Clemmensen, P.Johanson, H.Hod, R.Underwood, J.J.Bax, R.O.Bonow, F.Pinto, R.J.Gibbons, K.A.Fox, D.Atar, L.K.Newby, M.Galvani, C.W.Hamm, B.F.Uretsky, P.G.Steg, W.Wijns, J.P.Bassand, P.Menasché, J.Ravkilde, E.M.Ohman, E.M.Antman, L.C.Wallentin, P.W.Armstrong, M.L.Simoon, J.L.Januzzi, M.S.Nieminen,

M.Gheorghiade, G.Filippatos, R.V.Luepker, S.P.Fortmann, W.D.Rosamond, D.Levy, D.Wood, S.C.Smith, D.Hu, J.L.Lopez-Sendon, R.M.Robertson, D.Weaver, M.Tendera, A.A.Bove, A.N.Parkhomenko, E.J.Vasilieva, S.Mendis, H.Baumgartner, C.Ceconi, V.Dean, C.Deaton, R.Fagard, C.Funck-Brentano, D.Hasdai, A.Hoes, P.Kirchhof, J.Knuuti, P.Kolh, T.McDonagh, C.Moulin, B.A.Popescu, Ž.Reiner, U.Sechtem, P.A.Sirnes, A.Torbicki, A.Vahanian, S.Windecker, J.Morais, C.Aguiar, W.Almahmeed, D.O.Arnar, F.Barili, K.D.Bloch, A.F.Bolger, H.E.Bøtker, B.Bozkurt, R.Bugiardini, C.Cannon, J.DeLemos, F.R.Eberli, E.Escobar, M.Hlatky, S.James, K.B.Kern, D.J.Moliterno, C.Mueller, A.N.Neskovic, B.M.Pieske, S.P.Schulman, R.F.Storey, K.A.Taubert, P.Vranckx, D.R.Wagner, Third universal definition of myocardial infarction, Circulation. 126 (2012) 2020–2035. doi:10.1161/CIR.0b013e31826e1058.

[2] World Health Organization, WHO | Cardiovascular diseases (CVDs), Fact Sheets. (2017). http://www.who.int/mediacentre/factsheets/fs317/en/ (accessed August17, 2018).

[3] B.Ibanez, S.James, S.Agewall, M.J.Antunes, C.Bucciarelli-Ducci, H.Bueno, A.L.P.Caforio, F.Crea, J.A.Goudevenos, S.Halvorsen, G.Hindricks, A.Kastrati, M.J.Lenzen, E.Prescott, M.Roffi, M.Valgimigli, C.Varenhorst, P.Vranckx, P.Widimský, J.-P.Collet, S.D.Kristensen, V.Aboyans, A.Baumbach, R.Bugiardini, I.M.Coman, V.Delgado, D.Fitzsimons, O.Gaemperli, A.H.Gershlick, S.Gielen, V.-P.Harjola, H.A.Katus, J.Knuuti, P.Kolh, C.Leclercq, G.Y.H.Lip, J.Morais, A.N.Neskovic, F.-J.Neumann, A.Niessner, M.F.Piepoli, D.J.Richter, E.Shlyakhto, I.A.Simpson, P.G.Steg, C.J.Terkelsen, K.Thygesen, S.Windecker, J.L.Zamorano, U.Zeymer, S.Windecker, V.Aboyans, S.Agewall, E.Barbato, H.Bueno, A.Coca, J.-P.Collet, I.M.Coman, V.Dean, V.Delgado, D.Fitzsimons, O.Gaemperli, G.Hindricks, B.Iung, P.Jüni, H.A.Katus, J.Knuuti, P.Lancellotti, C.Leclercq, T.McDonagh, M.F.Piepoli, P.Ponikowski, D.J.Richter, M.Roffi, E.Shlyakhto, I.A.Simpson, J.L.Zamorano, M.Chettibi, H.G.Hayrapetyan, B.Metzler, F.Ibrahimov, V.Sujayeva, C.Beauloye, L.Dizdarevic-Hudic, K.Karamfiloff, B.Skoric, L.Antoniades, P.Tousek, P.J.Terkelsen, S.M.Shaheen, T.Marandi, M.Niemelä, S.Kedev, M.Gilard, A.Aladashvili, A.Elsaesser, I.G.Kanakakis, B.Merkely, T.Gudnason, Z.Iakobishvili, L.Bolognese, S.Berkinbayev, G.Bajraktari, M.Beishenkulov, I.Zake, H.BenLamin, O.Gustiene, B.Pereira, R.G.Xuereb, S.Ztot, V.Juliebø, J.Legutko, A.T.Timóteo, G.Tatu-Chiţoiu, A.Yakovlev, L.Bertelli, M.Nedeljkovic, M.Studenčan, M.Bunc, A.M.García de Castro, P.Petursson, R.Jeger, M.S.Mourali, A.Yildirir, A.Parkhomenko, C.P.Gale, 2017 ESC Guidelines for the management of acute myocardial infarction in patients presenting with ST-segment elevation, Eur. Heart J. 39 (2018) 119–177. doi:10.1093/eurheartj/ehx393.

[4] N.Tegn, M.Abdelnoor, L.Aaberge, K.Endresen, P.Smith, S.Aakhus, E.Gjertsen, O.Dahl-Hofseth, A.H.Ranhoff, L.Gullestad, B.Bendz, Invasive versus conservative strategy in patients aged 80 years or older with non-ST-elevation myocardial infarction or unstable angina pectoris (After Eighty study): an open-label randomised controlled trial, Lancet. 387 (2016) 1057–1065. doi:10.1016/S0140-6736(15)01166-6.

[5] L.Wallentin, L.Lindhagen, E.Ärnström, S.Husted, M.Janzon, S.P.Johnsen, F.Kontny, T.Kempf, L.-Å.Levin, B.Lindahl, M.Stridsberg, E.Ståhle, P.Venge, K.C.Wollert, E.Swahn, B.Lagerqvist, Early invasive versus non-invasive treatment in patients with non-ST-elevation acute coronary syndrome (FRISC-II): 15 year follow-up of a prospective, randomised, multicentre study, Lancet. 388 (2016) 1903–1911. doi:10.1016/S0140-6736(16)31276-4.

[6] M.A.Daubert, A.Jeremias, The utility of troponin measurement to detect myocardial infarction: Review of the current findings, Vasc. Health Risk Manag. 6 (2010) 691–699. doi:10.2147/VHRM.S5306.

[7] F.M.Asch, S.Shah, C.Rattin, S.Swaminathan, A.Fuisz, J.Lindsay, Lack of sensitivity of the electrocardiogram for detection of old myocardial infarction: a cardiac magnetic resonance imaging study., Am. Heart J. 152 (2006) 742–8. doi:10.1016/j.ahj.2006.02.037.

[8] J.Phillips, M.M.Miller, T.S.Mehta, V.Fein-Zachary, A.Nathanson, W.Hori, R.Monahan-Earley, P.J.Slanetz, Contrast-enhanced spectral mammography (CESM) versus MRI in the high-risk screening setting: patient preferences and attitudes, Clin. Imaging. 42 (2017) 193–197. doi:10.1016/J.CLINIMAG.2016.12.011.

[9] M.Saeed, T.A.Van, R.Krug, S.W.Hetts, M.W.Wilson, Cardiac MR imaging: current status and future direction., Cardiovasc. Diagn. Ther. 5 (2015) 290–310. doi:10.3978/j.issn.2223-3652.2015.06.07.

[10] V.S.Mahajan, P.Jarolim, How to interpret elevated cardiac troponin levels., Circulation. 124 (2011) 2350–4. doi:10.1161/CIRCULATIONAHA.111.023697.

[11] D.A.Morrow, M.P.Bonaca, Real-world application of “delta” troponin: Diagnostic and prognostic implications, J. Am. Coll. Cardiol. 62 (2013) 1239–1241. doi:10.1016/j.jacc.2013.06.049.

[12] J.Boeddinghaus, T.Nestelberger, R.Twerenbold, K.Wildi, P.Badertscher, J.Cupa, T.Bürge, P.Mächler, S.Corbière, K.Grimm, M.R.Giménez, C.Puelacher, S.Shrestha, D.Flores Widmer, J.Fuhrmann, P.Hillinger, Z.Sabti, U.Honegger, N.Schaerli, N.Kozhuharov, K.Rentsch, Ò.Miró, B.López, F.J.Martin-Sanchez, E.Rodriguez-Adrada, B.Morawiec, D.Kawecki, E.Ganovská, J.Parenica, J.Lohrmann, W.Kloos, A.Buser, N.Geigy, D.I.Keller, S.Osswald, T.Reichlin, C.Mueller, Direct Comparison of 4 Very Early Rule-Out Strategies for Acute Myocardial Infarction Using High-Sensitivity Cardiac Troponin IClinical Perspective, Circulation. 135 (2017) 1597–1611. doi:10.1161/CIRCULATIONAHA.116.025661.

[13] J.Boeddinghaus, T.Nestelberger, R.Twerenbold, P.Badertscher, M.Rubini Gimenez, K.Wildi, N.Schaerli, C.Puelacher, T.Reichlin, C.Mueller, 54Direct comparison of the ESC 0/3h-algorithm with four very early rule-out strategies for acute myocardial infarction using high-sensitivity cardiac troponin I, Eur. Heart J. 38 (2017). doi:10.1093/eurheartj/ehx501.54.

[14] H.Yokoyama, T.Higuma, T.Endo, F.Nishizaki, K.Hanada, T.Yokota, M.Yamada, K.Okumura, H.Tomita, "30-minute-delta" of high-sensitivity troponin I improves diagnostic performance in acute myocardial infarction, J. Cardiol. 71 (2018) 144–148. doi:10.1016/J.JJCC.2017.08.003.

[15] F.S.Apple, P.O.Collinson, IFCC Task Force on Clinical Applications of Cardiac Biomarkers, Analytical Characteristics of High-Sensitivity Cardiac Troponin Assays, Clin. Chem. 58 (2012) 54–61. doi:10.1373/clinchem.2011.165795.

[16] E.Giannitsis, H.A.Katus, Pros and cons of high-sensitivity assays for cardiac troponin, Nat. Rev. Cardiol. 9 (2012) 616–618. doi:10.1038/nrcardio.2012.142.

[17] T.Liu, L.L.Liang, P.Xiao, L.P.Sun, Y.Y.Huang, Y.Ran, L.Jin, B.O.Guan, A label-free cardiac biomarker immunosensor based on phase-shifted microfiber Bragg grating, Biosens. Bioelectron. 100 (2018) 155–160. doi:10.1016/j.bios.2017.08.061.

[18] N.Banterle, E.A.Lemke, Nanoscale devices for linkerless long-term single-molecule observation, Curr. Opin. Biotechnol. 39 (2016) 105–112. doi:10.1016/j.copbio.2016.02.013.

[19] M.M.Billingsley, R.S.Riley, E.S.Day, Antibody-nanoparticle conjugates to enhance the sensitivity of ELISA-based detection methods, PLoS One. 12 (2017) e0177592. doi:10.1371/journal.pone.0177592.

[20] A.Ambrosi, F.Airò, A.Merkoçi, Enhanced Gold Nanoparticle Based ELISA for a Breast Cancer Biomarker, Anal. Chem. 82 (2010) 1151–1156. doi:10.1021/ac902492c.

[21] J.Ikbal, G.S.Lim, Z.Gao, The hybridization chain reaction in the development of ultrasensitive nucleic acid assays, TrAC - Trends Anal. Chem. 64 (2015) 86–99. doi:10.1016/j.trac.2014.08.014.

[22] X.Ding, W.Cheng, Y.Li, J.Wu, X.Li, Q.Cheng, S.Ding, An enzyme-free surface plasmon resonance biosensing strategy for detection of DNA and small molecule based on nonlinear hybridization chain reaction, Biosens. Bioelectron. 87 (2017) 345–351. doi:10.1016/J.BIOS.2016.08.077.

[23] H.BinSeo, M.B.Gu, Aptamer-based sandwich-type biosensors, J. Biol. Eng. 11 (2017) 1–7. doi:10.1186/s13036-017-0054-7.

[24] H.-M.Chan, L.-S.Chan, R.N.-S.Wong, H.-W.Li, Direct Quantification of Single-Molecules of MicroRNA by Total Internal Reflection Fluorescence Microscopy, Anal. Chem. 82 (2010) 6911–6918. doi:10.1021/ac101133x.

[25] X.J.Feng, P.L.Wu, F.Bolze, H.W.C.Leung, K.F.Li, N.K.Mak, D.W.J.Kwong, J.-F.Nicoud, K.W.Cheah, M.S.Wong, Cyanines as New Fluorescent Probes for DNA Detection and Two-Photon Excited Bioimaging, Org. Lett. 12 (2010) 2194–2197. doi:10.1021/ol100474b.

[26] S.Ho, D.Xu, M.Shing, H.Li, Direct and Multiplex Quantification of Protein Biomarkers in Serum Sample with Immuno-magnetic Platform, Chem. Sci. 7 (2016) 2695-2700. doi:10.1039/C5SC04115E.

[27] P.Xie, L.Zhu, X.Shao, K.Huang, J.Tian, W.Xu, L.D.Varbanets, E.A.Zdorovenko, E.G.Garkavaya, O.S.Brovarskaya, G.Pieretti, S.Carillo, K.K.Kim, H.Otto, S.Drago, C.Anje, R.Elke, J.Ben, B.Peter, M.R.Pedersen, E.W.Hansen, J.D.Christensen, F.Mark, P.Jonathan, B.Joanne, J.D.Miller, K.U.Alwis, D.K.Milton, M.Yao, W.Qiang, Z.Zhu, W.Wu, J.Zhang, M.Zheng, M.Zuo, V.B.Kandimalla, X.J.Huang, W.Su, L.Q.Zhang, H.S.Sang, L.Yao, F.Gao, H.Chen,

L.A.Zheleznaya, T.A.Perevyazov, E.N.Zheleznyakov, N.I.Matvienko, W.Gao, D.C.Appleyard, S.C.Chapin, P.S.Doyle, R.M.Dirks, N.A.Pierce, W.Song, K.Zhu, Z.Cao, J.G.Bruno, M.P.Carrillo, T.Phillips, D.Mann, C.Reinemann, R.Stoltenburg, R.I.Bouças, H.T.Lanyon, K.V.Sandeep, E.M.Schneider, L.Edmond, H.J.Sabahudin, H.T.Luong, C.K.Dixit, S.K.Vashist, B.D.MacCraith, R.O'Kennedy, S.K.Vashist, M.Saraswat, H.Holthofer, S.Iijima, Highly sensitive detection of lipopolysaccharides using an aptasensor based on hybridization chain reaction, Sci. Rep. 6 (2016) 29524. doi:10.1038/srep29524.

[28] H.Jo, H.Gu, W.Jeon, H.Youn, J.Her, S.-K.Kim, J.Lee, J.H.Shin, C.Ban, Electrochemical Aptasensor of Cardiac Troponin I for the Early Diagnosis of Acute Myocardial Infarction, Anal. Chem. 87 (2015) 9869–9875. doi:10.1021/acs.analchem.5b02312.

[29] P.Venge, N.Johnston, B.Lindahl, S.James, Normal Plasma Levels of Cardiac Troponin I Measured by the High-Sensitivity Cardiac Troponin I Access Prototype Assay and the Impact on the Diagnosis of Myocardial Ischemia, J. Am. Coll. Cardiol. 54 (2009) 1165–1172. doi:10.1016/j.jacc.2009.05.051.

[30] Y.Sandoval, S.W.Smith, A.Sexter, S.E.Thordsen, C.A.Bruen, M.D.Carlson, K.W.Dodd, B.E.Driver, Y.Hu, K.Jacoby, B.K.Johnson, S.A.Love, J.C.Moore, K.Schulz, N.L.Scott, F.S.Apple, Type 1 and 2 Myocardial Infarction and Myocardial Injury: Clinical Transition to High-Sensitivity Cardiac Troponin I, Am. J. Med. 130 (2017) 1431–1439.e4. doi:10.1016/J.AMJMED.2017.05.049.

[31] M.Rubini Gimenez, P.Badertscher, R.Twerenbold, J.Boeddinghaus, T.Nestelberger, D.Wussler, O.Miro, J.Martin-Sanchez, T.Reichlin, C.Mueller, P5595Clinical effect of sex-specific cutoff values of high-sensitivity cardiac troponin I in suspected myocardial infarction, Eur. Heart J. 39 (2018). doi:10.1093/eurheartj/ehy566.P5595.

[32] A.S.VShah, M.Griffiths, K.K.Lee, D.A.McAllister, A.L.Hunter, A.VFerry, A.Cruikshank, A.Reid, M.Stoddart, F.Strachan, S.Walker, P.O.Collinson, F.S.Apple, A.J.Gray, K.A.A.Fox, D.E.Newby, N.L.Mills, High sensitivity cardiac troponin and the under-diagnosis of myocardial infarction in women: prospective cohort study, BMJ. 350 (2015) g7873. doi:10.1136/bmj.g7873.

[33] B.Zethelius, L.Berglund, J.Sundström, E.Ingelsson, S.Basu, A.Larsson, P.Venge, J.Ärnlöv, Use of Multiple Biomarkers to Improve the Prediction of Death from Cardiovascular Causes, N. Engl. J. Med. 358 (2008) 2107–2116. doi:10.1056/NEJMoa0707064.

[34] B.Zethelius, N.Johnston, P.Venge, Troponin I as a Predictor of Coronary Heart Disease and Mortality in 70-Year-Old Men: A Community-Based Cohort Study, Circulation. 113 (2006) 1071–1078. doi:10.1161/CIRCULATIONAHA.105.570762.